

Electromagnetically induced moiré optical lattices in a coherent atomic gas

Zhiming Chen,^{1,2,3} Xiuye Liu,^{1,4} and Jianhua Zeng^{1,4,*}

¹State Key Laboratory of Transient Optics and Photonics,

Xi'an Institute of Optics and Precision Mechanics of Chinese Academy of Sciences, Xi'an 710119, China

²School of Science, East China University of Technology, Nanchang 330013, China

³Collaborative Innovation Center of Light Manipulations and Applications, Shandong Normal University, Jinan 250358, China

⁴University of Chinese Academy of Sciences, Beijing 100049, China

(Dated: February 24, 2022)

Electromagnetically induced optical (or photonic) lattices via atomic coherence in atomic ensembles have recently received great theoretical and experimental interest. We here conceive a way to generate electromagnetically induced moiré optical lattices—a twisted periodic pattern when two identical periodic patterns (lattices) are overlapped in a twisted angle (θ)—in a three-level coherent atomic gas working under electromagnetically induced transparency. We show that, changing the twisted angle and relative strength between the two constitutive sublattices, the moiré Bloch bands that are extremely flattened can always appear, resembling the typical flat-band and moiré physics found in other contexts. Dynamics of light propagation in the induced periodic structures demonstrating the unique linear localization and delocalization properties are also revealed. Our scheme can be implemented in a Rubidium atomic medium, where the predicted moiré optical lattices and flattened bands are naturally observable.

Keywords electromagnetically induced transparency, moiré optical lattices, extremely flat bands, light propagation, coherent atomic gas

I. INTRODUCTION

Spatial periodic structures, particularly the man-made ones like waveguide arrays, photonic crystals and lattices, as well as optical lattices, have great applications in controlling the flow of light and matter waves because of their intriguing structural properties (e.g., partial and full photonic band gaps, symmetry-protected topological spectrum) [1–11]. The fabrications of such artificial periodic structures and investigations of the peculiar wave properties have been receiving great research attention in past years. Of particular interest in the optics and photonic communities are the two fabricated methods, direct femtosecond-laser writing technique and optically induced ones, with the former being widely used in solid materials where the induced photonic lattices have a permanent refractive index (and the optical and thermal stability of the laser machining method should be carefully processed) and the latter applies both to solid materials and gaseous media. The periodic structures manufactured by the latter method are aliased as electromagnetically induced gratings (EIGs), which are being extensively studied from both theoretical and experimental sides [12–23] in recent years, owing to the highly tunable degree of freedom of the induced periodic structures enabled by external and real-time changeable environments for both hot atomic vapours under room temperature and ultracold atoms (like Bose-Einstein condensates) in the nano-Kelvin regime.

Electromagnetically induced transparency (EIT) is a unique quantum interference in coherent atomic ensembles with multilevel electronic structures, where a strong control (light) field dresses the field-coupled states and then a weak probe

field cannot feel the absorption, leading to the cancellation of strong absorption completely in the induced transparency's spectral region and thus making the atomic medium transparent [24]. Interesting properties and promising futuristic applications that are closely associated with the EIT in an all-optical way include (but are not limited to) coherent population trapping, greatly enhanced nonlinear susceptibility, steep dispersion, slow and fast light, shape-stable coupled excitations of light and matter (the so-called dark-state polaritons), light storage (including nonlinear wave localization), communications and computations in both classic and quantum regimes [25–38]. Particularly worth mentioning is the fact that, the EIGs with tunable optical properties (lattice depth, periodicity, structural arrangement, etc.) under EIT regime are pushing towards the realization of those application targets [12–23].

In very recent years, scientists are progressing toward the realization of novel periodic structures, and particularly moiré patterns [39, 40]—two-dimensional (2D) twisted structures of two identical periodic structures overlapped in a twisted angle (θ)—are entering the optics and photonics communities while their fabrication by means of EIGs in gaseous medium still remains blank. Here a realizable all-optically way depended on the aforementioned optically induced technique for fabricating the moiré optical lattices in a three-level Λ -type atomic system under EIT is conceived. Rich and interesting extremely flat bands of the underlying band-gap structures are discovered for the electromagnetically induced moiré optical lattices, showing unique linear localization and delocalization moiré physics for light propagation as displayed in other 2D moiré structures reported elsewhere [39].

* zengjh@opt.ac.cn

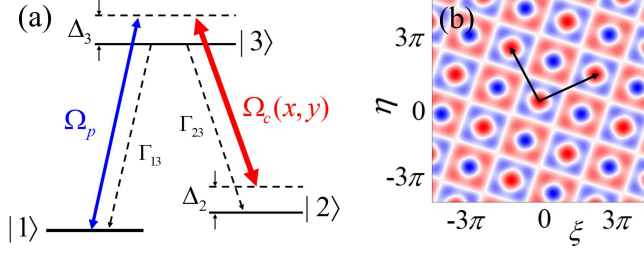


FIG. 1. (Color online) (a) Theoretical configuration of a Λ -type three-level atomic system that induces moiré optical lattices under EIT. A weak probe field Ω_p couples the ground state $|1\rangle$ to the excited state $|3\rangle$, and a strong space-dependent control field Ω_c couples the metastable state $|2\rangle$ to the excited state $|3\rangle$. The spontaneous emission decay rates of transitions $\Gamma_{13, 23}$ and detunings $\Delta_{2, 3}$ are defined in the text. The combined effect of weak probe and strong control fields, Ω_p and Ω_c , kindles the standard EIT regime. (b) Contour plot of the spatial periodic modulated control field $\Omega_c(x, y)$ that is taken as a moiré pattern (shaded blue, pattern minima; shaded red, pattern maxima) at $\epsilon_1 = \epsilon_2 = 1$ with rotation angle $\theta = \arctan(3/4)$. The black arrows denote the primitive vectors.

II. THEORETICAL MODEL

Our fundamental theory relates to light propagation in a three-level Λ -type coherent atomic ensemble working in EIT regime, as described in Fig. 1(a). A weak probe field with half-Rabi frequency Ω_p and center angular frequency ω_p dresses ground state $|1\rangle$ to excited state $|3\rangle$, and a very strong continuous-wave control field with half-Rabi frequency Ω_c and center angular frequency ω_c , modulated periodically in spatial, connects metastable state $|2\rangle$ to excited state $|3\rangle$. The spontaneous emission decay rates of transitions $|3\rangle \rightarrow |1\rangle$ and $|3\rangle \rightarrow |2\rangle$ are represented by Γ_{13} and Γ_{23} , and the detunings $\Delta_2 = \omega_p - \omega_c - \omega_{21}$ and $\Delta_3 = \omega_p - \omega_{31}$, here $\omega_{j1} = (E_j - E_1)/\hbar$ with E_j being the eigen energy of state $|j\rangle$. To obtain the electromagnetically induced moiré optical lattices under the EIT condition, the control field (after simplification) is chosen as the periodic function of spatial coordinates (x, y) , i.e.,

$$\Omega_c(x, y) = \Omega_{c0}[1 + f(x, y)]. \quad (1)$$

Here Ω_{c0} is a constant describing the magnitude of the control field, and $f(x, y) = \epsilon_1(\cos^2 x + \cos^2 y) + \epsilon_2(\cos^2 x' + \cos^2 y')$, $\epsilon_{1,2} > 0$ being the modulation depth (amplitude) of the two optical lattices with the same periodicity π . The rotated (x', y') plane at a rotating angle θ yields

$$\begin{pmatrix} x' \\ y' \end{pmatrix} = \begin{pmatrix} \cos \theta & -\sin \theta \\ \sin \theta & \cos \theta \end{pmatrix} \begin{pmatrix} x \\ y \end{pmatrix}. \quad (2)$$

For discussion, we define the strength contrast as $p = \epsilon_1/\epsilon_2$. The contour plot of the control field $\Omega_c(x, y)$ given by Eq. (1) taken as moiré square lattice is displayed in Fig. 1(b), showing a spatial twisted displacement compared to the conventional square lattice.

By adopting the standard Maxwell-Bloch equations that describe the propagation of probe field Ω_p , and after substitution

as detailed in [Supplement Information](#), we have the dimensionless 2D envelope equation

$$i \frac{\partial u}{\partial s} = -\frac{1}{2} \left(\frac{\partial^2}{\partial \xi^2} + \frac{\partial^2}{\partial \eta^2} \right) u + V_{\text{OL}}(\mathbf{r})u, \quad (3)$$

where the dimensionless variables are defined as spatial coordinates $\mathbf{r} = (\xi, \eta) = (x, y)/R$, $u = \Omega_p/U_0$, and propagation distance $s = z/L_{\text{Diff}}$ with typical diffraction length $L_{\text{Diff}} = \omega_p R^2/c$. Here U_0 and R are the typical Rabi frequency and beam radius of the probe field. The coefficient of the last term in Eq. (3) represents the induced moiré optical lattice potential with lattice depth V_0 [See [Supplement Information](#)]

$$V_{\text{OL}}(\mathbf{r}) = -\frac{V_0}{[1 + f(\xi, \eta)]^2}. \quad (4)$$

The theoretical model considered here can be realized in realistic physical systems. Specifically, the energy levels $|1\rangle$, $|2\rangle$, and $|3\rangle$ can be selected respectively as $5^2S_{1/2}(F = 1)$, $5^2S_{1/2}(F = 2)$, and $5^2P_{1/2}(F = 2)$ states of ^{87}Rb atoms tuned to D1-line transition [41], and the decay rates are given by $\Gamma_2 \simeq 1.0$ kHz, and $\Gamma_3 \simeq 5.75$ MHz, and $|\mathbf{p}_{13}| = 2.54 \times 10^{-27}$ C cm. To achieve the dimensionless 2D envelope equation (3), other parameters are chosen as $\mathcal{N}_a = 3.69 \times 10^{10} V_0 \text{ cm}^{-3}$ (V_0 is a real constant denoting lattice depth), $\Omega_{c0} = 1.0 \times 10^7$ Hz, $R = 36 \mu\text{m}$, $\Delta_1 = 0$, $\Delta_2 = 1.0 \times 10^5$ Hz, and $\Delta_3 = 1.0 \times 10^4$ Hz, and thus the typical diffraction length is $L_{\text{Diff}} = 1.0$ cm. Note that these parameters are used in all our calculations reported below.

III. NUMERICAL RESULTS

We stress that once again the electromagnetically induced moiré optical lattices [given in Eq. (4)] provide a rotational degree of freedom for the periodic structures, in contrast to those conventional periodic optical patterns formed also under the EIT condition. As pointed out elsewhere [42], when Pythagorean angle is satisfied, $\theta = \arctan(a/b)$, $\cos \theta = a/c$ and natural numbers (a, b, c) obey $a^2 + b^2 = c^2$, the moiré optical lattices Eq. (4) can be defined as periodic structures in the first Brillouin zone, and then the corresponding band gap structures can be easily obtained using the Bloch theory. To this end, the probe field u can be written as $u = U(\mathbf{r}) \exp(i\beta s)$, where β is the propagation constant, and the stationary envelope $U(\mathbf{r})$ can be sought as the form $U(\mathbf{r}) = \phi_{\mathbf{k}}(\mathbf{r}) \exp(i\mathbf{k} \cdot \mathbf{r})$, here the wave vectors $\mathbf{k} = (k_x, k_y)$ are confined to the first reduced Brillouin zone of the moiré optical lattices, and $\phi_{\mathbf{k}}(\mathbf{r}) = \phi_{\mathbf{k}}(\mathbf{r} + \mathbf{d})$ is a periodic Bloch function having the same periodicity \mathbf{d} as the lattices. Then the dispersion relation of the 2D Bloch waves, $\beta(\mathbf{k})$, can be found by calculating the linear eigenvalue problem

$$\left[\frac{1}{2} \left(\frac{\partial}{\partial \mathbf{r}} + i\mathbf{k} \right)^2 - V_{\text{OL}}(\mathbf{r}) \right] \phi_{\mathbf{k}}(\mathbf{r}) = \beta(\mathbf{k})\phi_{\mathbf{k}}(\mathbf{r}). \quad (5)$$

Numerically, we adopt the plane wave expansion method [2] to calculate the eigenvalue problem (5), periodic boundary

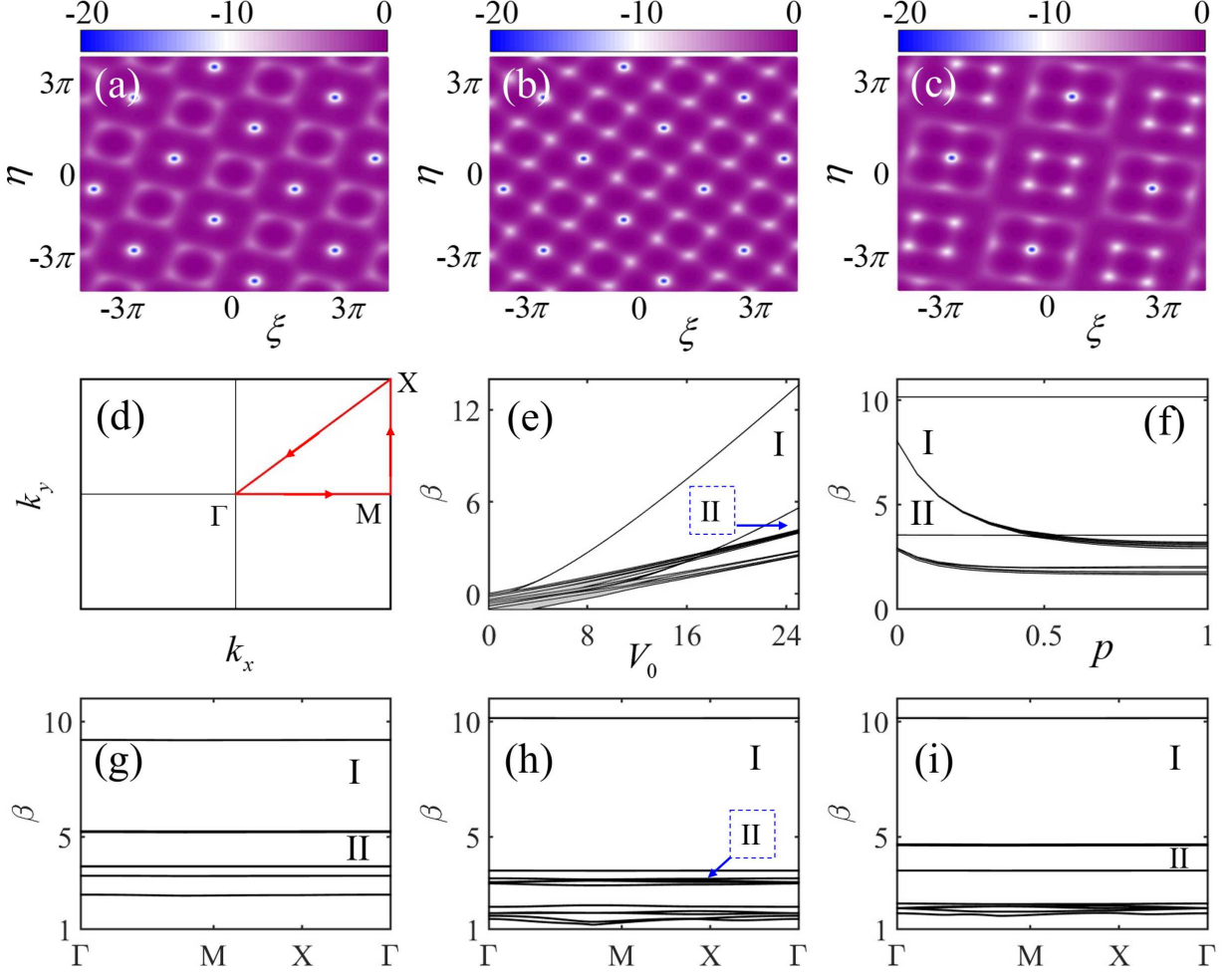


FIG. 2. Contour shapes of the electromagnetically induced moiré optical lattice potentials (shaded blue, potential minima; shaded purple, potential maxima) with different parameters: (a) twisted angle $\theta = \arctan(3/4)$ and strength contrast $p = 1$ ($\epsilon_1 = \epsilon_2 = 1$), (b) $\theta = \arctan(3/4)$ and $p = 0.25$ ($\epsilon_1 = 0.4, \epsilon_2 = 1.6$), (c) $\theta = \arctan(5/12)$ and strength contrast $p = 1$. We have set $V_0 = 20$ for panels (a)-(c). (d) The first Brillouin zone of the induced lattice potentials in the reciprocal space; signed are high symmetry points (Γ , M, X). The linear Bloch-wave spectra (expressed by propagation constant β) of the induced optical lattice at twisted angle $\theta = \arctan(3/4)$ with (e) varying V_0 and $p = 1$, (f) different ratios p and $V_0 = 20$. Band-gap structures of the lattices at $p = 1$ and $V_0 = 20$ and under different twisted angles: (g) $\theta = \arctan(3/4)$ and (h) $\theta = \arctan(5/12)$. (i) Band-gap structure with $p = 0.25$ and $V_0 = 20$ at $\theta = \arctan(3/4)$. I and II in panels (e)-(i) represent the first and second finite band gaps, respectively.

condition is applied based on the Bloch theory. Such processing way is matured in optics context for processing photonic crystals, more details could be referred to Ref. [2].

Figures 2(a)~2(c) display the shapes of the induced moiré optical lattices under different Pythagorean angles θ and strength contrast as $p = \epsilon_1/\epsilon_2$ with $V_0 = 20$. To calculate the associated band gap structures, we have given the first Brillouin zone in the momentum (reciprocal) space (k_x, k_y) in Fig. 2(d), whose exact values can be tuned to portray the electromagnetically induced moiré lattice potentials with varying twisted angles θ . The linear band-gap structures of the lattices, described as propagation constant β versus lattice depth V_0 and versus strength contrast p ($= \epsilon_1/\epsilon_2$), are respectively displayed in Figs. 2(e) and 2(f). It is observed from the former that the width of the first finite band gap widens and more higher band gaps emerge with an increase of V_0 . At $V_0 = 20$

while increasing p , the first finite band gap widens while the second gap narrows, according to the latter. The rich spectra (and the variation rule with changing V_0 and p) of the moiré lattice potentials in Figs. 2(e) and 2(f) supplement and enrich the band-gap properties of the moiré patterns in other optics backgrounds [39, 40, 42], implying the possibility of finding flat band feature of the induced lattices in our model.

At a defined V_0 and p , the underlying band-gap structures of the induced moiré lattice potentials change dramatically with different twisted angle θ , comparing the Figs. 2(g) and 2(h); interestingly, there are a lot of flattened bands, which are a unique feature of moiré patterns [39, 40, 42]. One can see that at $\theta = \arctan(3/4)$, there exists a wide first band gap and the second gap is in a moderate width; keeping other conditions constant while setting $\theta = \arctan(5/12)$, a much wider first gap is created and the second gap shrinks greatly. The

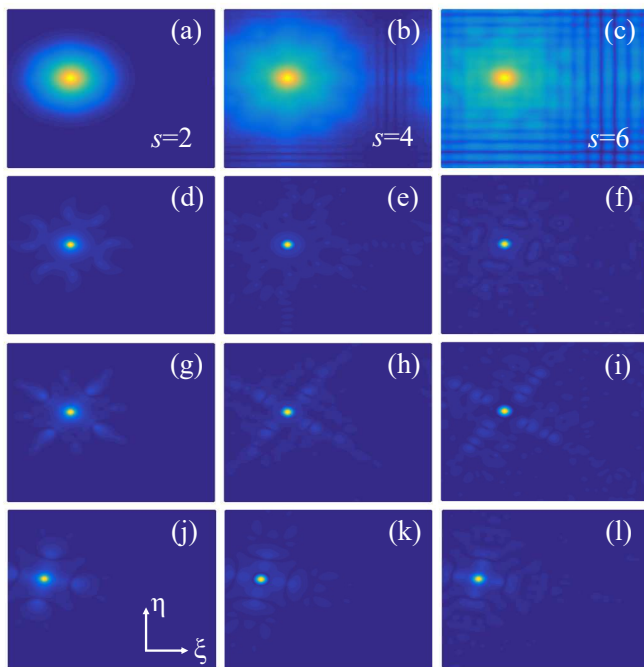


FIG. 3. Linear propagations of light (module, $|u|$) in the induced moiré optical lattices at twisted angle $\theta = \arctan(3/4)$ and different propagation distance s ($s = z/L_{\text{Diff}}$, as given below the Eq. (3)) displaying delocalization [(a)~(c)] and localization [(d)~(f), (g)~(i)] properties. Other parameters: (a)~(c) strength contrast $p = 1$, lattice depth $V_0 = 1$; (d)~(f) $p = 1$, $V_0 = 20$; (g)~(i) $p = 0.25$, $V_0 = 20$. (j)~(l) show the linear propagations of light in the induced moiré optical lattices at twisted angle $\theta = \arctan(5/12)$ with $p = 1$, $V_0 = 20$ for the light propagating to $s = 2$, $s = 4$, and $s = 6$, respectively. $\xi, \eta \in [-12, 12]$ for all panels.

strength contrast p is also an important parameter that can change the band-gap structure of the induced moiré lattices, through changing it, the widths of the first finite band gap and the second one can be tuned almost by will, according to Fig. 2(i) and as compared with Fig. 2(g). As emphasized above, the electromagnetically induced periodic structures have a tunable advantage, since the power, structural arrangement, and dimensionality of the laser fields could be modulated based on the experimental requirements; in this respect, not only the moiré square lattices described here, but also the moiré aperiodic lattices and the hitherto unexplored spectrum property can also be envisaged, which will be the future direction.

The most recent theoretical predictions and experimental progresses of moiré lattices in optics community have proven the spectacular linear localization mechanism provided by the flat bands of the lattice [39, 43]. It is thus natural to ask whether such new localization paradigm or regime can be complied with in our electromagnetically induced moiré optical lattices. Our answer is a definitely yes. Figure 3 demonstrates such linear localization and delocalization properties of light propagation in the moiré optical lattices introduced

here when it propagates to $s = 2, 4, 6$, respectively. Under delocalization paradigm, light propagation in the moiré lattice undergoes the typical diffraction pattern along the propagation distance, as seen in Figs. 3(a)~3(c) for such evolutions at twisted angle $\theta = \arctan(3/4)$ with strength contrast $p = 1$ and lattice depth $V_0 = 1$; under the localization regime offered by the flat bands, both the shape and strength of the input light could be well conserved, as displayed by two typical examples in the second line and the third one of Fig. 3 at twisted angle $\theta = \arctan(3/4)$ and $V_0 = 20$ with $p = 1$ and $p = 0.25$, respectively. It is seen that the localized light in Figs. 3(g)~3(i) has more weak side patterns compared to that of Figs. 3(d)~3(f), this difference is induced by the different configurations of the moiré optical lattices (as comparing the Figs. 2(a) and 2(b)), apparently, there is a stronger Bragg diffraction since the existence of several higher sublattices around the lattice minima for the case of $p = 0.25$. We also demonstrate that the twisted angle of the moiré optical lattices has a great impact on the light propagation, figures 3(j)~3(l) display the linear propagations of light at twisted angle $\theta = \arctan(5/12)$ with $p = 1$ and $V_0 = 20$, which reveals that the shape and position of light change as the twisted angle changes in the localization and delocalization mechanisms. It is relevant to mention that the light evolutions in Fig. 3 are produced by means of both the fast-Fourier transform and fourth-order Runge-Kutta methods, and both methods can smoothly match. The initial light input we used is the 2D Gaussian beam with appropriate amplitude and waist.

IV. CONCLUSION

Summarizing, we have conceived a way to generate 2D moiré lattice potentials in a coherent atomic ensemble using the optically (electromagnetically) induced method. We find that the lattice depth V_0 , twisted angle θ , and strength contrast p could have great influences on the shapes and the band-gap structures of the resulting moiré lattice potentials, emphasizing the flat band property. The extraordinary localization and delocalization abilities of the induced moiré lattice are also confirmed. Considering the fact that our theoretical analyses are based on the realistic atomic media with realizable parameters, the predicted electromagnetically induced moiré lattices and the associated moiré physics can be readily observed in experiments. Future research interests may be paid attention to the moiré aperiodic lattices at non-Pythagorean angles θ and in nonlinear situation where the nonlinear localization of light in atomic gases is yet to be explored.

Electronic supplementary material Electronic supplementary materials are available in the online version of this article at <https://> and <http://> and are accessible for authorized users.

Acknowledgments This work was supported by the National Natural Science Foundation of China (11704066, 12074423, 12074063), and Jiangxi Provincial Natural Science Foundation (20202BABL211013).

-
- [1] Y. S. Kivshar and G. P. Agrawal, *Optical solitons: From fibers to photonic crystals*, San Diego: Academic Press, 2003.
- [2] J. D. Joannopoulos, S. G. Johnson, J. N. Winn, and R. D. Meade, *Photonic Crystals: Molding the Flow of Light*, 2nd ed., Princeton: Princeton University Press, 2011.
- [3] O. Morsch and M. Oberthaler, Dynamics of Bose-Einstein condensates in optical lattices, *Rev. Mod. Phys.* **78**(1), 179 (2006).
- [4] I. L. Garanovich, S. Longhi, A. A. Sukhorukova, and Y. S. Kivshar, Light propagation and localization in modulated photonic lattices and waveguides, *Phys. Rep.* **518**(1-2), 1 (2012).
- [5] Y. V. Kartashov, G. E. Astrakharchik, B. A. Malomed, and L. Torner, Frontiers in multidimensional self-trapping of nonlinear fields and matter, *Nat. Rev. Phys.* **1**(3), 185 (2019).
- [6] L. Zeng and J. Zeng, Gap-type dark localized modes in a Bose-Einstein condensate with optical lattices, *Adv. Photon.* **1**(4), 046004 (2019).
- [7] L. Zeng and J. Zeng, Preventing critical collapse of higher-order solitons by tailoring unconventional optical diffraction and nonlinearities, *Commun. Phys.* **3**(1), 26 (2020).
- [8] J. Shi and J. Zeng, Self-trapped spatially localized states in combined linear-nonlinear periodic potentials, *Front. Phys.* **15**(1), 12602 (2020).
- [9] Y.-Y. Zheng, S.-T. Chen, Z.-P. Huang, S.-X. Dai, B. Liu, Y.-Y. Li, and S.-R. Wang, Quantum droplets in two-dimensional optical lattices, *Front. Phys.* **16**(2), 22501 (2021).
- [10] J. Li and J. Zeng, Dark matter-wave gap solitons in dense ultracold atoms trapped by a one-dimensional optical lattice, *Phys. Rev. A* **103**(1), 013320 (2021).
- [11] J. Chen and J. Zeng, Dark matter-wave gap solitons of Bose-Einstein condensates trapped in optical lattices with competing cubic-quintic nonlinearities, *Chaos, Solitons & Fractals* **150**, 111149 (2021).
- [12] Y. Zhang, Z. Wu, M. R. Belić, H. Zheng, Z. Wang, M. Xiao, and Y. Zhang, Photonic Floquet topological insulators in atomic ensembles, *Laser Photonics Rev.* **9**(3), 331 (2015).
- [13] F. Wen, H. Ye, X. Zhang, W. Wang, S. Li, H. Wang, Y. Zhang, and C.-W. Qiu, Optically induced atomic lattice with tunable near-field and far-field diffraction patterns, *Photon. Res.* **5**(6), 676 (2017).
- [14] F. Wen, X. Zhang, H. Ye, W. Wang, H. Wang, Y. Zhang, Z. Dai, and C.-W. Qiu, Efficient and Tunable Photoinduced Honeycomb Lattice in an Atomic Ensemble, *Laser Photonics Rev.* **12**(9), 1800050 (2018).
- [15] L. Zhao, Electromagnetically induced polarization grating, *Sci. Rep.* **8**(1), 3073 (2018).
- [16] C. Hang, W. Li, and G. Huang, Nonlinear light diffraction by electromagnetically induced gratings with \mathcal{PT} symmetry in a Rydberg atomic gas, *Phys. Rev. A* **100**(4), 043807 (2019).
- [17] Z. Zhang, F. Li, G. Malpuech, Y. Zhang, O. Bleu, S. Koniakhin, C. Li, Y. Zhang, M. Xiao, and D. D. Solnyshkov, Particlelike behavior of topological defects in linear wave packets in photonic graphene, *Phys. Rev. Lett.* **122**(23), 233905 (2019).
- [18] J. Yuan, C. Wu, L. Wang, G. Chen, and S. Jia, Observation of diffraction pattern in two-dimensional optically induced atomic lattice, *Opt. Lett.* **44**(17), 4123 (2019).
- [19] H. Zhang, J. Yuan, S. Dong, C. Wu, and L. Wang, Observation of an Electromagnetically Induced Grating in Cold ^{85}Rb Atoms, *Appl. Sci.* **10**(17), 5740 (2020).
- [20] Z. Zhang, R. Wang, Y. Zhang, Y. V. Kartashov, F. Li, H. Zhong, H. Guan, K. Gao, F. Li, Y. Zhang, and M. Xiao, Observation of edge solitons in photonic graphene, *Nat. Commun.* **11**(1), 1902 (2020).
- [21] Z. Zhang, Y. Shen, S. Ning, S. Liang, Y. Feng, C. Li, Y. Zhang, and M. Xiao, Transport of light in a moving photonic lattice via atomic coherence, *Opt. Lett.* **46**(17), 4096 (2021).
- [22] S. Ning, J. Lu, S. Liang, Y. Feng, C. Li, Z. Zhang, and Y. Zhang, Talbot effect of an electromagnetically induced square photonic lattice assisted by a spatial light modulator, *Opt. Lett.* **46**(19), 5035 (2021).
- [23] Z. Shi and G. Huang, Selection and cloning of periodic optical patterns with a cold Rydberg atomic gas, *Opt. Lett.* **46**(21), 5344 (2021).
- [24] M. Fleischhauer, A. Imamoğlu, and J. P. Marangos, Electromagnetically induced transparency: Optics in coherent media, *Rev. Mod. Phys.* **77**(2), 633 (2005).
- [25] M. Fleischhauer and M. D. Lukin, Dark-State Polaritons in Electromagnetically Induced Transparency, *Phys. Rev. Lett.* **84**(22), 5094 (2000).
- [26] C. Liu, Z. Dutton, C. H. Behroozi, and L. V. Hau, Observation of coherent optical information storage in an atomic medium using halted light pulses, *Nature (London)* **409**(6819), 490 (2001).
- [27] M. D. Lukin and A. Imamoğlu, Controlling photons using electromagnetically induced transparency, *Nature (London)* **413**(6853), 273 (2001).
- [28] A. André and M. D. Lukin, Manipulating light pulses via dynamically controlled photonic band gap, *Phys. Rev. Lett.* **89**(14), 143602 (2002).
- [29] C. Hang, G. Huang, and V. V. Konotop, \mathcal{PT} Symmetry with a System of Three-Level Atoms, *Phys. Rev. Lett.* **110**(8), 083604 (2013).
- [30] Z. Chen, Z. Bai, H. Li, C. Hang, and G. Huang, Storage and retrieval of (3+1)-dimensional weak-light bullets and vortices in a coherent atomic gas, *Sci. Rep.* **5**(1), 08211 (2015).
- [31] D. Xu, Z. Chen, and G. Huang, Ultraslow weak-light solitons and their storage and retrieval in a kagome-structured hollow-core photonic crystal fiber, *Opt. Express* **25**(16), 19094 (2017).
- [32] K. Zhang, Y. Liang, J. Lin, and H. Li, Controlling the stability of nonlinear optical modes via electromagnetically induced transparency, *Phys. Rev. A* **97**(2), 023844 (2018).
- [33] Z. Chen, H. Xie, Q. Li, and G. Huang, Stern-Gerlach deflection of optical Thirring solitons in a coherent atomic system, *Phys. Rev. A* **100**(1), 013827 (2019).
- [34] Z. Bai, W. Li, and G. Huang, Stable single light bullets and vortices and their active control in cold Rydberg gases, *Optica* **6**(3), 309 (2019).
- [35] J. Ru, Z. Wu, Y. Zhang, F. Wen, and Y. Gu, Talbot effect in nonparaxial self-accelerating beams with electromagnetically induced transparency, *Front. Phys.* **15**(5), 52503 (2020).
- [36] J. Tang, Y. Deng, and C. Lee, Tunable photon blockade with a single atom in a cavity under electromagnetically induced transparency, *Photon. Res.* **9**(7), 1226 (2021).
- [37] Z. Chen and J. Zeng, Localized gap modes of coherently trapped atoms in an optical lattice, *Opt. Express* **29**(3), 3011 (2021).
- [38] Z. Chen and J. Zeng, Two-dimensional optical gap solitons and vortices in a coherent atomic ensemble loaded on optical lattices, *Commun. Nonlinear Sci. Numer. Simulat.* **102**, 105911 (2021).
- [39] P. Wang, Y. Zheng, X. Chen, C. Huang, Y. V. Kartashov, L. Torner, V. V. Konotop, and F. Ye, Localization and delocalization of light in photonic moiré lattices, *Nature (London)*

- 577(7788), 422 (2020).
- [40] Q. Fu, P. Wang, C. Huang, Y. V. Kartashov, L. Torner, V. V. Konotop, and F. Ye, Optical soliton formation controlled by angle twisting in photonic moiré lattices, *Nat. Photon.* **14**(11), 663 (2020).
- [41] D. A. Steck, Rubidium 87 D Line Data. <http://steck.us/alkalidata> (revision 2.2.2, 9 July 2021).
- [42] C. Huang, F. Ye, X. Chen, Y. V. Kartashov, V. V. Konotop, and L. Torner, Localization-delocalization wavepacket transition in Pythagorean aperiodic potentials, *Sci. Rep.* **14**(1), 663 (2016).
- [43] X.-R. Mao, Z.-K. Shao, H.-Y. Luan, S.-L. Wang, and R.-M. Ma, Magic-angle lasers in nanostructured moiré superlattice, *Nat. Nanotechnol.* **16**(10), 1099 (2021).

Supplementary Information for “Electromagnetically induced moiré optical lattices in a coherent atomic gas”

Zhiming Chen,^{1,2,3} Xiuye Liu,^{1,4} and Jianhua Zeng^{1,4,*}

¹*State Key Laboratory of Transient Optics and Photonics,*

Xi'an Institute of Optics and Precision Mechanics of Chinese Academy of Sciences, Xi'an 710119, China

²*School of Science, East China University of Technology, Nanchang 330013, China*

³*Collaborative Innovation Center of Light Manipulations and Applications, Shandong Normal University, Jinan 250358, China*

⁴*University of Chinese Academy of Sciences, Beijing 100049, China*

(Dated: February 24, 2022)

This supplementary documents provide further details on deriving the envelope equation that governs the fundamental theory of creating electromagnetically induced moiré optical lattices in the main text. In Sec. **I**, we describe the physical model under consider and give the explicit expressions of the underlying Maxwell-Bloch equations. We show the derivation of the two-dimensional envelope equation in Sec. **II**.

arXiv:2202.11275v1 [physics.optics] 23 Feb 2022

* zengjh@opt.ac.cn

I. MAXWELL-BLOCH EQUATIONS

We consider light propagation in a three-level Λ -type coherent atomic ensemble that is cooled to an ultralow temperature to eliminate the Doppler broadening effect [1] [See Fig. 1(a) in the main text]. A weak probe field with half-Rabi frequency Ω_p and center angular frequency ω_p couples ground state $|1\rangle$ to excite state $|3\rangle$, and a very strong continuous-wave control field with half-Rabi frequency Ω_c and center angular frequency ω_c , modulated periodically in spatial, bridges metastable state $|2\rangle$ to excite state $|3\rangle$. The spontaneous emission decay rates of transitions $|3\rangle \rightarrow |1\rangle$ and $|3\rangle \rightarrow |2\rangle$ are represented by Γ_{13} and Γ_{23} , and the detunings $\Delta_2 = \omega_p - \omega_c - \omega_{21}$ and $\Delta_3 = \omega_p - \omega_{31}$, here $\omega_{jl} = (E_j - E_l)/\hbar$ with E_j being the eigen energy of state $|j\rangle$. It should be noted that, in reality, the energy levels $|1\rangle$, $|2\rangle$, and $|3\rangle$ can be selected respectively as $5^2S_{1/2}(F=1)$, $5^2S_{1/2}(F=2)$, and $5^2P_{1/2}(F=2)$ states of ^{87}Rb atoms tuned to D1-line transition [2]. Under an appropriate condition, the two laser fields and the atomic gas result in a well-known EIT core where the absorption of the probe field can be suppressed remarkably due to the quantum interference effect induced by the control field [3]. To obtain the electromagnetically induced moiré optical lattices under the EIT condition, the control field (after simplification) is chosen as the periodic function of spatial coordinates (x, y) [See the main text].

In our model, both the probe and control laser fields are assumed to propagate along the z direction, thus the electric-field vector can be written as $\mathbf{E} = \mathbf{E}_p + \mathbf{E}_c = \hat{\mathbf{e}}_p \mathcal{E}_p e^{i(k_p z - \omega_p t)} + \hat{\mathbf{e}}_c \mathcal{E}_c(x, y) e^{i(k_c z - \omega_c t)} + \text{c.c.}$. Here $\hat{\mathbf{e}}_p$ ($\hat{\mathbf{e}}_c$) is the unit vector of the probe (control) field with the envelope \mathcal{E}_p (\mathcal{E}_c), ω_p (ω_c) is the angular frequency of the probe (control) field, and $k_p = \omega_p/c$ ($k_c = \omega_c/c$) is the wavenumber of the probe (control) field before entering the atomic gas. Under the methods of electric-dipole and rotating-wave approximations, the Hamiltonian of the system in the interaction picture is

$$\hat{\mathcal{H}}_{\text{int}} = - \sum_{j=1}^3 \hbar \Delta_j |j\rangle \langle j| - \hbar [\Omega_c |3\rangle \langle 2| + \Omega_p |3\rangle \langle 1| + \text{H.c.}], \quad (\text{S1})$$

with $\Delta_1 = 0$. Here $\Omega_c = (\mathbf{p}_{23} \cdot \hat{\mathbf{e}}_c) \mathcal{E}_c / \hbar$ and $\Omega_p = (\mathbf{p}_{13} \cdot \hat{\mathbf{e}}_p) \mathcal{E}_p / \hbar$ are half Rabi frequencies of the control and probe fields, where \mathbf{p}_{jl} is the electric dipole matrix element related to the transition from $|j\rangle$ to $|l\rangle$. Thus the equation of motion for density matrix σ in the interaction picture is given by

$$i \frac{\partial}{\partial t} \sigma_{11} - i \Gamma_{13} \sigma_{33} + \Omega_p^* \sigma_{31} - \Omega_p \sigma_{31}^* = 0, \quad (\text{S2a})$$

$$i \frac{\partial}{\partial t} \sigma_{22} - i \Gamma_{23} \sigma_{33} + \Omega_c^* \sigma_{32} - \Omega_c \sigma_{32}^* = 0, \quad (\text{S2b})$$

$$i \frac{\partial}{\partial t} \sigma_{33} + i(\Gamma_{13} + \Gamma_{23}) \sigma_{33} - \Omega_p^* \sigma_{31} + \Omega_p \sigma_{31}^* - \Omega_c^* \sigma_{32} + \Omega_c \sigma_{32}^* = 0, \quad (\text{S2c})$$

$$\left(i \frac{\partial}{\partial t} + d_{21} \right) \sigma_{21} - \Omega_p \sigma_{32}^* + \Omega_c^* \sigma_{31} = 0, \quad (\text{S2d})$$

$$\left(i \frac{\partial}{\partial t} + d_{31} \right) \sigma_{31} - \Omega_p (\sigma_{33} - \sigma_{11}) + \Omega_c \sigma_{21} = 0, \quad (\text{S2e})$$

$$\left(i \frac{\partial}{\partial t} + d_{32} \right) \sigma_{32} - \Omega_c (\sigma_{33} - \sigma_{22}) + \Omega_p \sigma_{21}^* = 0, \quad (\text{S2f})$$

where $d_{jl} = \Delta_j - \Delta_l + i\gamma_{jl}$. Dephasing rates are defined as $\gamma_{jl} = (\Gamma_j + \Gamma_l)/2 + \gamma_{jl}^{\text{col}}$ with $\Gamma_j = \sum_{E_i < E_j} \Gamma_{ij}$ being the spontaneous emission rate from the state $|j\rangle$ to all lower energy states $|i\rangle$ and γ_{jl}^{col} being the dephasing rate reflecting the loss of phase coherence between $|j\rangle$ and $|l\rangle$.

According to the method of slowly varying envelope approximation, the Maxwell equation for the probe-field Rabi frequency Ω_p is described as [4]

$$i \left(\frac{\partial}{\partial z} + \frac{1}{c} \frac{\partial}{\partial t} \right) \Omega_p + \frac{c}{2\omega_p} \left(\frac{\partial^2}{\partial x^2} + \frac{\partial^2}{\partial y^2} \right) \Omega_p + \frac{\omega_p}{2c} \chi_p \Omega_p = 0, \quad (\text{S3})$$

where $\chi_p = \mathcal{N}_a |\mathbf{p}_{13} \cdot \hat{\mathbf{e}}_p|^2 \sigma_{31} / (\hbar \varepsilon_0 \Omega_p)$ is the optical susceptibility of the probe field, with \mathcal{N}_a being atomic density. Because we focus on the stationary state of the system under study, we assume that the time duration of the probe field is very large, i.e., the time derivatives in the Maxwell-Bloch Eqs. (S2) and (S3) can be neglected appropriately.

II. DERIVATION OF ENVELOPE EQUATION

To investigate electromagnetically induced moiré optical lattices in the linear circumstance, we assume that the intensity of probe field is very weak. Thus the Bloch Eq. (S2) can be solved by using a perturbation expansion, i.e., Ω_p being taken as a small parameter. The linear solution of nondiagonal element is read as

$$\sigma_{31} = \frac{d_{21}\Omega_p}{|\Omega_c|^2 - d_{21}d_{31}}. \quad (\text{S4})$$

Based on this solution we can achieve the expression of the optically induced susceptibility of the probe field with the form [5, 6]

$$\chi_p = \frac{\mathcal{N}_a |\mathbf{p}_{13} \cdot \hat{\mathbf{e}}_p|^2}{\hbar \varepsilon_0} \frac{d_{21}}{|\Omega_c|^2 - d_{21}d_{31}}. \quad (\text{S5})$$

Because of the energy levels being selected from ^{87}Rb atoms tuned to D1-line transition, the decay rates are given by $\Gamma_2 \simeq 1.0$ kHz, and $\Gamma_3 \simeq 5.75$ MHz, and $\mathbf{p}_{13} = 2.54 \times 10^{-27}$ C cm [2]. Through choosing other parameters $\mathcal{N}_a = 3.69 \times 10^{10} V_0 \text{ cm}^{-3}$ (V_0 is a real constant), $\Omega_{c0} = 1.0 \times 10^7$ Hz, $R = 36 \mu\text{m}$, $\Delta_1 = 0$, $\Delta_2 = 1.0 \times 10^5$ Hz, and $\Delta_3 = 1.0 \times 10^4$ Hz, the real part and the imaginary part of product term $d_{21}d_{31}$ are much smaller than $|\Omega_{c0}|^2$. In addition, we introduce some dimensionless variables: spatial coordinates $\mathbf{r} = (\xi, \eta) = (x, y)/R$, $u = \Omega_p/U_0$, and propagation distance $s = z/L_{\text{Diff}}$ with typical diffraction length $L_{\text{Diff}} = \omega_p R^2/c$. Here U_0 and R are the typical Rabi frequency and beam radius of the probe field. Based on the parameters mentioned above, we can obtain the typical diffraction length $L_{\text{Diff}} = 1.0$ cm. Then the Maxwell equation for the probe-field Rabi frequency can be convert into the dimensionless 2D envelope equation

$$i \frac{\partial u}{\partial s} = -\frac{1}{2} \left(\frac{\partial^2}{\partial \xi^2} + \frac{\partial^2}{\partial \eta^2} \right) u + V_{\text{OL}}(\mathbf{r})u, \quad (\text{S6})$$

The coefficient of the last term in Eq. (S6) represents the induced moiré optical lattice potential with lattice depth V_0

$$V_{\text{OL}}(\mathbf{r}) = -\frac{V_0}{[1 + f(\xi, \eta)]^2}. \quad (\text{S7})$$

-
- [1] Z. Chen and J. Zeng, Two-dimensional optical gap solitons and vortices in a coherent atomic ensemble loaded on optical lattices, *Commun. Nonlinear Sci. Numer. Simulat.* **102**, 105911 (2021).
- [2] D. A. Steck, Rubidium 87 D Line Data. <http://steck.us/alkalidata> (revision 2.2.2, 9 July 2021).
- [3] M. Fleischhauer, A. Imamoglu, and J. P. Marangos, Electromagnetically induced transparency: Optics in coherent media, *Rev. Mod. Phys.* **77**(2), 633 (2005).
- [4] L. Qin, C. Hang, and G. Huang, Controllable \mathcal{PT} phase transition and asymmetric soliton scattering in atomic gases with linear and nonlinear potentials, *Phys. Rev. A* **99**(4), 043832 (2019).
- [5] Z. Zhang, F. Li, G. Malpuech, Y. Zhang, O. Bleu, S. Koniakhin, C. Li, Y. Zhang, M. Xiao, and D. D. Solnyshkov, Particlelike behavior of topological defects in linear wave packets in photonic graphene, *Phys. Rev. Lett.* **122**(23), 233905 (2019).
- [6] Z. Zhang, R. Wang, Y. Zhang, Y. V. Kartashov, F. Li, H. Zhong, H. Guan, K. Gao, F. Li, Y. Zhang, and M. Xiao, Observation of edge solitons in photonic graphene, *Nat. Commun.* **11**(1), 1902 (2020).